Molecular dynamics simulation of the interfacial thermal resistance between phosphorene and silicon substrate

Jingchao Zhang [a], Yang Hong [b], Mengqi Liu [c], Yanan Yue [d], Qingang Xiong [e,*], Giulio Lorenzini [f,*]

[a] Holland Computing Center, University of Nebraska-Lincoln, Lincoln, NE, 68588, USA
[b] Department of Chemistry, University of Nebraska-Lincoln, Lincoln, NE 68588, USA
[c] T-Rex Engineering + Construction, Houston, TX 77015, USA
[d] School of Power and Mechanical Engineering, Wuhan University, Wuhan, Hubei 430072, China
[e] Oak Ridge National Laboratory, Oak Ridge, TN 37831, USA
[f] Department of Industrial Engineering, University of Parma, 43124 Parma, Italy

ARTICLE INFO

ABSTRACT

Phosphorene is a recently discovered member of the two-dimensional (2D) monolayer materials, which has been reported to exhibit unique characteristics on mechanical and thermal properties. This study is the first time to show the exceptional thermal conductance between phosphorene and crystalline silicon substrate through classical molecular dynamics (MD) simulations. MD simulations revealed that under conventional conditions, the interfacial thermal resistance (R) between phosphorene and silicon is very low and independent on the thickness (h) of silicon substrate when h is larger than 3.12 nm. It was also found that R decreases remarkably with the increases in system temperature (T_{ie}) and contact strength (χ). To further explicitly display the superiority of phosphorene on interfacial heat transfer, R of other two popular 2D monolayer materials, i.e., graphene and silicene, were calculated for comparison. The comparisons revealed that R of phosphorene shows two distinct advantages over graphene and silicene. On one hand, within the studied ranges of T_{ie} and χ, R between phosphorene and silicon substrate is about quarter of that between graphene and silicon substrate, which proves that phosphorene is really a high-performance 2D monolayer material for interfacial heat transfer. On the other hand, with the increases in T_{ie} and χ, R between phosphorene and silicon substrate decreases more sharply than that between silicene and silicon substrate, indicating that phosphorene is more sensitive to environmental variations.

1. Introduction

The novel structure that monolayer atoms are aligned with honeycomb lattice has brought two-dimensional (2D) materials such as graphene and silicene many distinguished thermo-physical properties compared to traditional materials. One of the remarkable properties these 2D monolayer materials possess is their rather low interfacial thermal resistance for heat dissipation into adjacent substrates, which makes them as appealing candidates for the design of next-generation nano-devices [1–5]. Phosphorene, a newly synthesized 2D monolayer material, has attracted great interest in recent years due to its novel structural and electronic properties, e.g., layer-dependent direct bandgaps and high electron/hole mobility [6–8]. It has been reported that

phosphorene-based field-effect transistors exhibit very high carrier mobility and extraordinary on/off ratios [9–11], which show its great potential to be applied to high-performance nano-electronic devices. However, whether phosphorene is also outstanding on interfacial heat transfer still remains unclear.

Because of the extremely small spatiotemporal scales, existing experimental approaches still face inherent challenges in accurate measurement of thermal properties for 2D monolayer materials, including interfacial thermal resistance. In recent years, with the dramatic increases in computational power, classical molecular dynamics (MD) simulation which directly resolves thermal properties at atomistic scale, has been widely used in the investigation of 2D monolayer materials. Thermal conductivity, thermal rectification as well as interfacial thermal resistance of 2D monolayer materials, have been extensively studied by MD simulations [12–17]. These MD simulations, to a large extent, complement experimental approaches to quantitatively clarify the novel thermal properties of 2D monolayer materials, especially those of graphene

* Corresponding authors.
E-mail addresses: qgxiong@126.com (Q. Xiong), giulio.lorenzini@unipr.it (G. Lorenzini).

and silicene. These MD studies have contributed significantly to our knowledge on the thermal behaviors of 2D materials, ranging from fundamental to application levels.

So far, to the best of our knowledge, MD simulations of interfacial thermal resistance for 2D monolayer materials have not been applied to phosphorene. This is majorly because compared with other 2D monolayer materials, until recently the key parameters to quantitatively determine interactions among atoms within phosphorene, such as cut-off distances and bonding angles, have not been available. The lack of such key parameters has largely hindered the utilization of the powerful MD technology to study the interfacial thermal resistance of phosphorene. Very recently, using the valence force field model [18], Wu accurately determined those parameters required by the Stillinger–Weber (SW) potential [19]. Those first-principle calculated parameters have been proved to be accurate when applied to model the mechanical properties [20,21] and thermal conductivity of phosphorene [22,23] and phosphorus nanotubes [24]. Therefore, the way to successful MD simulation of the interfacial thermal resistance for phosphorene has been paved by those precise first-principle calculated parameters.

In most nano-devices, silicon is used as substrate to support 2D monolayer materials for heat dissipation. Therefore, it is highly desirable to characterize the interfacial heat transfer between phosphorene and silicon. This study explored the interfacial thermal resistance between phosphorene and crystalline silicon substrate by MD simulations with the SW potential using the foregoing mentioned precise first-principle calculated parameters. A transient pump–probe technique mimicking the experimental thermo-reflectance method was applied to evaluate the interfacial thermal resistance. To comprehensively demonstrate the characteristics of the interfacial thermal resistance between phosphorene and silicon substrate, cases with graphene and silicene contacting silicon substrate were also included for comparison. In the following, the physical models and computational setup are first described. Then, the characteristics of interfacial thermal resistance between phosphorene and silicon substrate are presented. The effects of substrate thickness, system temperature and coupling strength on the interfacial thermal resistance are explored. Finally, the superiority of phosphorene on interfacial thermal resistance compared to graphene and silicene is discussed.

2. Numerical models

In a typical MD simulation, the most important aspect is to have an appropriate inter-atom potential. It should be not only physi-

cally accurate but also computationally economic. In this study, the classical Tersoff potential was chosen to model the interactions among silicon atoms [25] as

$$E = \frac{1}{2}\sum_i \sum_{j\neq i} f_c(r_{ij})\left[f_R(r_{ij}) + b_{ij}f_A(r_{ij})\right], \tag{1}$$

where E is the three-body system energy, and $f_c(r_{ij})$ is the cutoff function to limit the range of the potential since the short-range interaction can save great computational effort. The function $f_R(r_{ij})$ represents the repulsive pair potential, which includes the orthogonalization energy when atomic wave functions overlap, and $f_A(r_{ij})$ is an attractive pair potential associated with bonding. The b_{ij} term is a monotonically decreasing function of the coordination of atoms i and j. Detailed information on classical Tersoff potential can be found in Ref. [25]. It has been proved by many prior MD studies that the micro-scale behaviors for silicon can be successfully reproduced by the classical Tersoff potential [26–28]. As mentioned above, the interactions among phosphorene atoms were modeled by the SW potential as follows

$$V_2 = Ae^{\left[\frac{\rho}{r-r_{max}}\right]}\left(\frac{B}{r^4} - 1\right), \tag{2}$$

$$V_3 = Ke^{\left[\frac{\rho_1}{r_{12}-r_{max12}} + \frac{\rho_2}{r_{13}-r_{max13}}\right]}(\cos\theta - \cos\theta_0)^2, \tag{3}$$

where V_2 and V_3 represent the two-body bond stretching and three-body angle bending interactions respectively. A and K the energy parameters and B, ρ_1, ρ_2, θ and θ_0 are the geometry parameters. These parameters were calculated by the first-principle valence force field model [18]. The cutoff distances r_{max}, r_{max12} and r_{max13} are determined by the lattice structures. Following our previous simulations [29], the coupling between silicon and phosphorene was modeled by the classical 12-6 Lennard–Jones potential as

$$V(r) = 4\chi\varepsilon_{P-Si}\left[\left(\frac{\sigma_{P-Si}}{r}\right)^{12} - \left(\frac{\sigma_{P-Si}}{r}\right)^6\right], \tag{4}$$

where r is the distance between silicon and phosphorene atoms. $\varepsilon_{P\text{-}Si}$, $\sigma_{P\text{-}Si}$, and χ are the depth of the potential well (eV), zero potential distance (Å), and coupling strength, respectively. It is worth noting that another popular approach to manipulate the coupling strength is to insert an interlayer at the interfaces [30–32]. In this study, the values of $\varepsilon_{P\text{-}Si}$ and $\sigma_{P\text{-}Si}$ were determined by the universal force field model [33], resulting in $\varepsilon_{P\text{-}Si}$ = 15.205 meV and $\sigma_{P\text{-}Si}$ = 3.760 Å. All the MD simulations in this study were performed on the LAMMPS Molecular Dynamics Simulator [34].

3. Computational setup

The simulation system is schematically shown in Fig. 1, where the red and green solid dots represent phosphorene and silicon atoms, respectively. Dimensions of the simulation domain are $10.87 \times 10.77 \times 3.76$ nm^3 in $x \times y \times z$ directions. Periodic boundary conditions were applied to the in-plane (x and y) directions to eliminate the size effect. Parametric studies showed that the calculated R is insensitive to the further increases in domain sizes in $x \times y$ directions. The free boundary condition was used in the out-of-plane (z) direction to avoid atom interactions through the upper and bottom boundaries. The phosphorene layer was initially placed 4.22 Å above the silicon substrate, and was allowed to freely conform to the substrate surface. It has been proved that such initial distance has a negligible effect on the equilibrium structures as long as it is within the cutoff radius of the empirical potentials [35]. The thickness of the silicon substrate (h) was varied from 3.12 nm to 5.97 nm and its effects on R will be discussed later. Time step was chosen to be 0.5 fs for all simulations.

A transient heating technique which has been used extensively for thermal characterization of micro- and nano-films [36–38] was employed in this study. This technique was conducted as follows. After the initial thermal equilibrium calculations when the system reaches its initial equilibrium temperature (T_{ie}), the supported 2D membrane is exposed to an ultrafast thermal impulse, which will cause a temperature rise in the monolayer system. Since the membrane is supported on the substrate in an enclosed space, the only heat pathway for the thermal energy dissipation is from the 2D layer to the substrate. Therefore, in the subsequent thermal relaxation process, the surface temperature of phosphorene will decrease due to the heat conduction to the substrate. The schematic diagram of the transient heating technique is shown in Fig. 2. Since periodic boundary conditions are applied to the lateral (x and y) directions, the phosphorene structure is repetitively expanded across the space. Therefore, the supported phosphorene
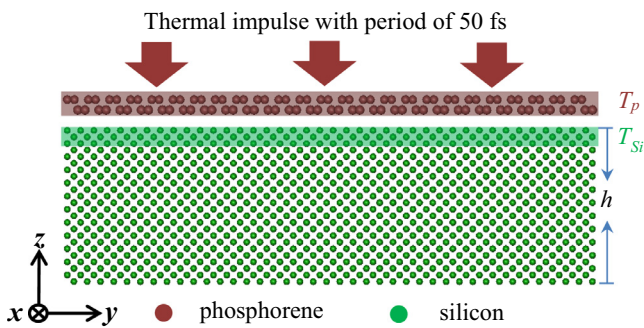

Fig. 1. Schematic diagram of the phosphorene and silicon hybrid system. Phosphorene energy (E_t), phosphorene temperature (T_p), and temperature of top three silicon layers (T_{Si}) were recorded each time step in the thermal relaxation process.
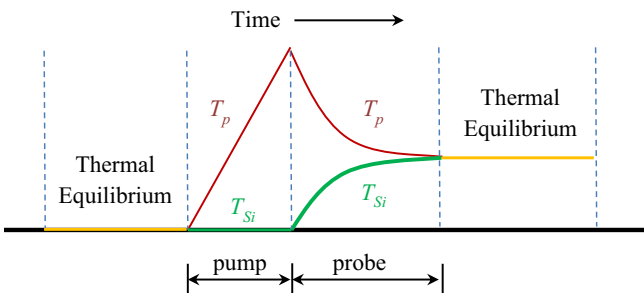

Fig. 2. Schematic diagram of the transient heating technique.
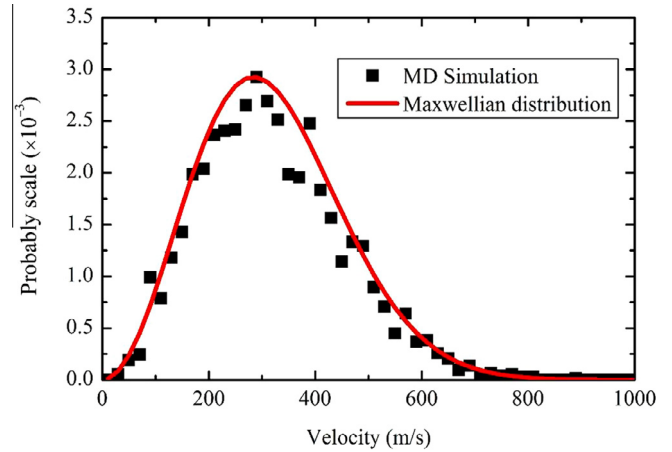

Fig. 3. Comparison of MD velocity with theoretical Maxwellian distribution.

should be considered as an 2D sheet, instead of 2D ribbon. Under such scenario, the imposed heat is applied to an infinite large phosphorene region. To further prove this statement, velocities of the phosphorene system at thermal equilibrium state are extracted and compared to the theoretical Maxwellian distribution. As shown in Fig. 3, a sound match is found between the MD velocities and theoretical predictions. Through its applications to the interfacial thermal transports in graphene/boron-nitride [35], graphene/silicon [29] and graphene/copper [39] systems, this transient heating technique has been demonstrated to be more effective than the traditional non-equilibrium approach which can introduce the undesired phonon scattering due to the localized heating and cooling.

4. Results and discussion

4.1. Characteristics of the phosphorene/silicon interfacial thermal resistance

Due to the temperature difference between phosphorene and silicon, both the energy and temperature of phosphorene should decrease and finally reach their steady state, as confirmed by the example shown in Fig. 4. In this case, the phosphorene/silicon system with T_{ie} = 250 K, h = 3.12 nm and χ = 1.0, was suddenly given a thermal impulse of $q_{in} = 4.68 \times 10^{-4}$ W to the phosphorene layer using the above-mentioned transient heating technique. At the end of such excitation, the temperatures of the adjacent layers for phosphorene and silicon were 387 K and 253 K. Then this temperature difference drove the heat transfer across the phosphorene/silicon interface. The temporal evolutions of energy of phosphorene (E_t), and the spatially averaged temperatures of the phosphorene (T_P) and the top three layers of silicon atoms (T_{Si}) were monitored for another 100 ps. As can be seen in Fig. 4, because of the interfacial heat transfer, E_t and T_P decreased, while T_{Si} increased, all finally reached their statistically steady states.

R can be calculated through the obtained E_t, T_P and T_{Si} as

$$\frac{\partial E_t}{\partial t} = \frac{A \cdot (T_P - T_{Si})}{R}, \tag{5}$$

where A is the interfacial area and t is the time instant after the end of excitation. The energy decay fitting in Fig. 4 is performed based on Eq. (5) and takes the integral form of $E_t = E_0 + (A/R) \cdot \int_0^t (T_P - T_{Si}) dt$. Here R is treated as a constant, and such assumption will be discussed and validated later. E_0 is phosphorene's initial energy. The change of E_t against $\int (T_P - T_{Si}) dt$ is plotted in Fig. 5(a). It can be seen that E_t almost decreases linearly
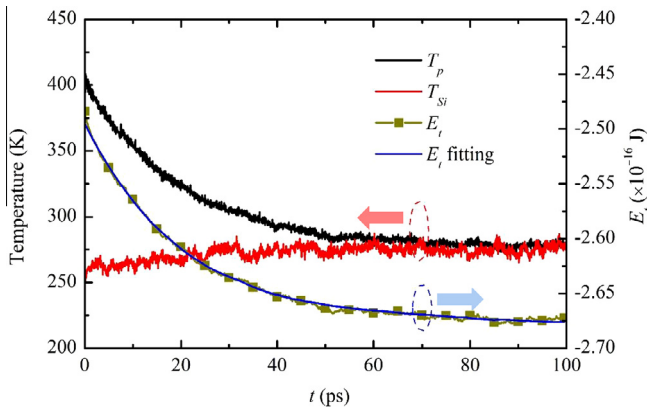
Fig. 4. Temporal evolutions of E_t, T_P, and T_{Si} after the heat impulse. T_{ie}, χ, and h were set to be 250 K, 1.0, and 3.12 nm, respectively. Blue solid line represents the fitting results based on the energy decay model. The red and blue arrows denote that the circled profiles represent temperature (left y axis) and energy (right y axis) values respectively. (For interpretation of the references to colour in this figure legend, the reader is referred to the web version of this article.)

with $\int(T_P - T_{Si})dt$, from which R can be determined by the slope. To investigate the temporal variation of R with t, the E_t curve was divided into segments as shown in Fig. 5(a). For each segment, R was obtained using the averaged slope. Variation of the calculated R with respect to t is shown in Fig. 5(b). It can be observed that at the later stage of interfacial heat transfer, R nearly remains constant. Therefore, in the following, R will be viewed as constant during the entire transient process. In this case, the obtained value of R is 1.63×10^{-8} K·m²/W.

Under ultrafast heating/cooling processes, the system's initial temperature evolutions will be different from the traditional heat dissipation phenomenon, which is normally referred to as the non-Fourier effects. The dynamic temperature responses under ultra-high-speed heating have shown some behaviors that could not be predicted by the thermal-diffusion theory and many models have been developed to interpret these experiments [40]. The transient pump–probe technique adopted in this work induces a non-Fourier effect which lasts for less than 1 ps, whereas the elapsed time for thermal resistance characterization is 100 ps. The small deviations at the initial stage will not change the overall fitting
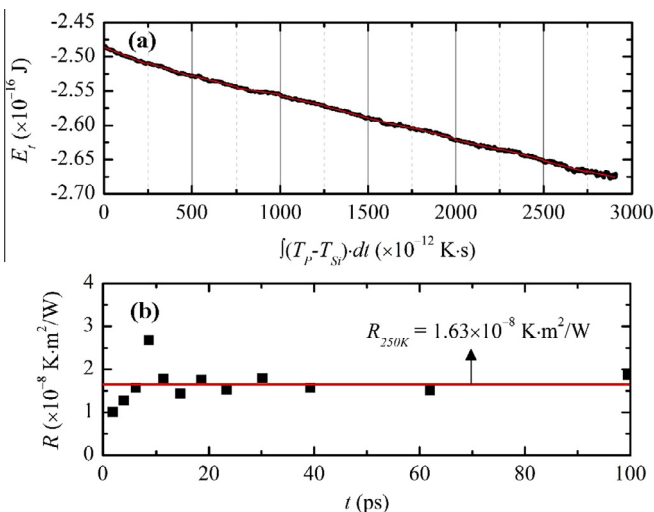
results. Therefore, the non-Fourier effects are not considered in the calculations.

The h used in a typical MD simulation is usually much smaller than those in experiments. Therefore, it is highly necessary to clarify the dependence of R on h. The variation of R with respect to h is shown in Fig. 6(a). For each value of h, five independent runs were performed to eliminate statistical errors. It can be observed that R is nearly irrelevant to the change of h. Thus, it can be concluded that the chosen h (3.12 nm) in the following is sufficient to quantitatively reproduce the interfacial thermal resistance between phosphorene and silicon. To further elaborate our understanding of the mechanisms on heat transfer within the silicon substrate, the temperature contours for the case with $h = 3.12$ nm are shown in Fig. 6(b). It can be seen that the temperature distribution along the thickness direction within the silicon substrate is nearly uniform during the last 50 ps. It is postulated that the independence of R on h is due to the weak thermal couplings at the phosphorene/silicon interface and the relatively high thermal conductivity of silicon. Therefore, in the following, h is chosen to be 3.12 nm for all simulations to reduce the computational cost.

The variation of R for phosphorene with respect to T_{ie} is shown in Fig. 7(a). It can be clearly seen that with the increases in T_{ie}, R decreases significantly. This indicates that at higher system temperature, the heat transfer across the phosphorene/silicon interface becomes elevated. The dependence of R on T_{ie} can be majorly explained by the phonon density of state (PDOS) of phosphorene at different temperatures. Generally, PDOS can be calculated by
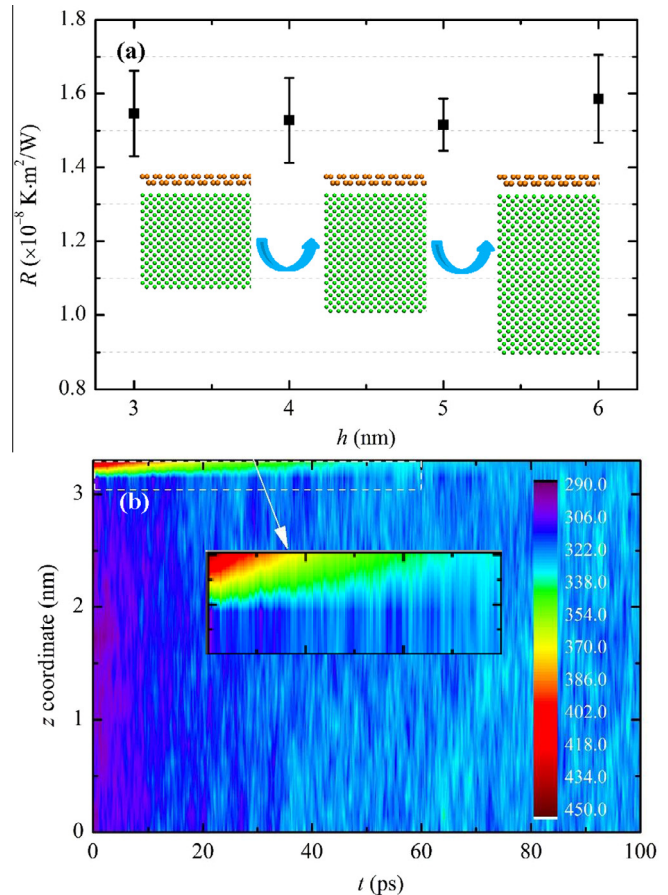
Fig. 6. (a) Effects of silicon thickness (h) on the interfacial thermal resistance. A maximum of 4.6% variation is calculated when the silicon thickness increases from 3.12 nm to 5.97 nm. The smallest value 3.12 nm is used in this work to reduce the computational cost. (b) Spatiotemporal evolutions of system temperature after the ultrafast heat impulse.

Fig. 5. (a) Energy relaxation profile of phosphorene can be correlated to $(T_P - T_{Si})dt$ by integrating the temperature differences between phosphorene and silicon. (b) Segment interfacial thermal resistance values calculated from (a) are around the overall fitting results.

taking the Fourier transform of the velocity autocorrelation function as

$$G(\omega) = \frac{1}{\sqrt{2\pi}} \int_{-\infty}^{\infty} Z(t) e^{i\omega t} dt, \tag{6}$$

where $Z(t) = < v(0) \cdot v(t) > / < v(0) \cdot v(0) >$. For a given ω, higher PDOS means more states are occupied by for a phonon, whereas zero PDOS means no phonon exists in the system. One of the crucial factors in determining the interfacial thermal resistance is the overlap of phonon states. If the phonon population for a certain ω is very low, the energy propagation by phonons of that wave vector will be highly restricted. Therefore, the variation of overlap area between the PDOS with respect to temperature needs to be explored. To quantify this variation, an arbitrary unit variable, defined as

$$\delta = \int \omega A(\omega) d\omega, \tag{7}$$

is introduced to help assist the analyses [41]. $A(\omega)$ represents the intersection area of PDOS at ω. The area integration is proportional to the amount of energy transported across the interface by phonons at these frequency intervals. To facilitate comparison of the differences between the calculated results, the integration area for each PDOS is normalized to unity. The calculated δ between phosphorene and silicon was found to increase from 0.56 to 0.83 as temperature increases from 150 K to 400 K. Increased δ values means higher phonon coupling rates at the interface, contributing to the lower interfacial thermal resistance. The calculated δ results at other temperatures are shown in Fig. 7(b), which demonstrate a monotonic increasing trend with temperature and further explain the decreasing of R in Fig. 7(a). Since the phonon frequency does not depend on the amplitude of the oscillations, the phonon density of states of harmonic systems should be temperature-independent. However, when the temperature increases to 400 K, it is observed that both the PDOS of phosphorene and Si become broader, which indicates that the umklapp scattering mechanism is dominant within this temperature range and the phonon anharmonicity is significant. The umklapp processes reduce the phonon mean free paths (MFP) on both sides of the interface and alter the PDOS distribution with more activated higher frequency phonons. Contributions from the high frequency phonons to thermal transport reduce the thermal contact resistance. Moreover, the three phonon scatterings become more furious at high temperatures, which will decompose the high frequency phonons into lower frequency branches and couple with the other phonons in the hybrid system, and as a result, the PDOS overlap value increases while the predicted R decreases.

In practical applications, the interfacial heat transfer can take place under various contact pressures.[42–44] Therefore, the variation of R for phosphorene with respect to χ was investigated and the results are shown in Fig. 8. In these simulations, T_{ie} was fixed at 250 K. It can be seen that a quite similar trend to that of T_{ie} is found for the variation of χ. Such behavior may be explained as follows. Compared with van der Waals bonding, the covalent bonding among thermal interface materials can greatly reduce the thermal contact resistance, which indicates the stronger interatomic interactions are more effective for phonon transport across the interfaces. The stronger coupling strength can enhance the phonon couplings at the interface, which directly contributes to the interfacial thermal transport and reduces R. It is worth noting that at liquid–solid interfaces, the variations of Kapitza length and coupling strength can be fitted with exponential functions, whereas it cannot be directly applied to the solid–solid interface studies in this work [45–48].
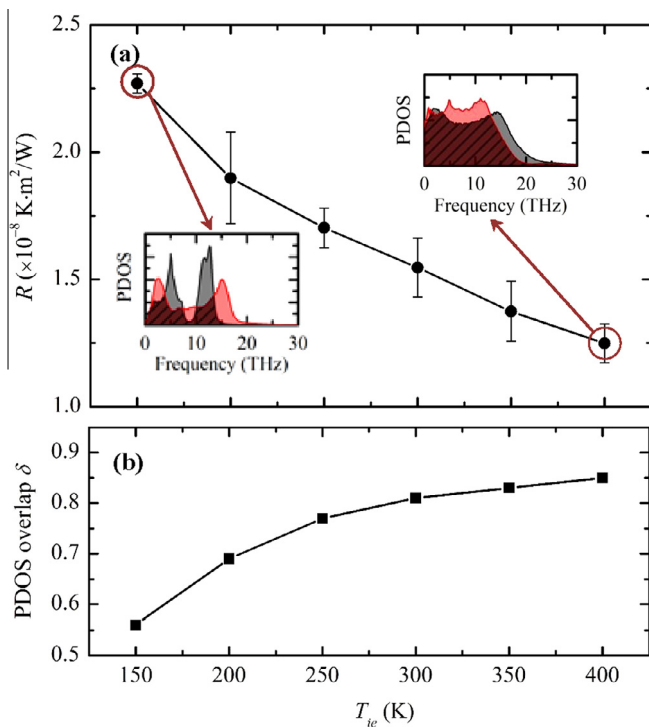
4.2. Comparative studies with graphene and silicene

To gain a clearer picture about the interfacial thermal resistance for phosphorene, comparative MD simulations on the interfacial heat transfer across graphene/silicon and silicene/silicon were conducted. Dimensions and boundary conditions of the graphene and silicene systems are the same as those of phosphorene. The second generation of the Brenner potential [49], reactive empirical bond-order (REBO), based on the Tersoff potential [25] for the interac-
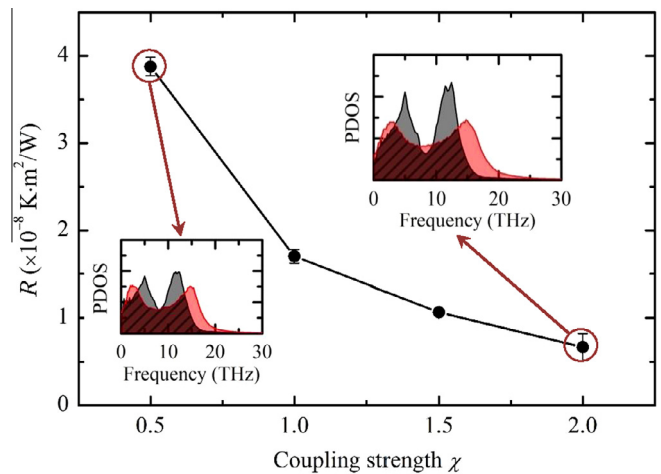

Fig. 7. (a) Temperature dependence of interfacial thermal resistance between phosphorene and silicon. Insets depict the phonon power spectra at temperatures 150 K and 400 K. The grey and red shaded areas represent phosphorene and silicon respectively. Each power spectrum profile is normalized to an integration area of unity. (b) PDOS overlap with system's equilibrium temperature. (For interpretation of the references to colour in this figure legend, the reader is referred to the web version of this article.)

Fig. 8. Dependence of interfacial thermal resistance between phosphorene and silicon on coupling strength. Insets depict the phonon power spectra when χ equals 0.5 and 2.0. The grey and red shaded areas represent phosphorene and silicon respectively. (For interpretation of the references to colour in this figure legend, the reader is referred to the web version of this article.)

tions between C–C bonds was employed to model the graphene system. The REBO potential was chosen because its functions and parameters have been proved to give reasonable predictions for the thermal properties of graphene [50]. The modified Tersoff potential by Kumagai et al. [51] was used to describe the silicene system, which was also used in our previous studies [52]. The interactions of graphene and silicene with silicon substrates were still modeled by the *12-6* Lennard–Jones potential. The energy and distance parameters between graphene and silicon were set as ε_{C-Si} = 8.909 meV and σ_{C-Si} = 3.326 Å [29], while for silicene and silicon they were set as ε_{Si-Si} = 17.440 meV and σ_{Si-Si} = 3.826 Å [52].

The variations of R for phosphorene, graphene and silicene with respect to T_{ie} are shown in Fig. 9. It can be clearly observed that, on one hand, R for phosphorene is about 1/4 of that for graphene. This means that under the same T_{ie}, phosphorene is better than graphene for interfacial heat transfer, although graphene already shows amazingly low interfacial thermal resistance. On the other hand, with the increases in T_{ie}, R for phosphorene decreases more remarkably than that for silicene, indicating that phosphorene is more sensitive to the change of environmental temperature. Likewise, within the studied range of χ, phosphorene owns much lower R than graphene and higher sensitivity than silicene, as shown in Fig. 10.

The reasons why phosphorene possesses much lower R than graphene at the same environmental conditions may be explained as follows. The out-of-plane phonons (ZA mode) in graphene are the main energy carriers during thermal transport [53]. According to previous studies on the interfacial thermal transport across graphene and adjacent material, the phonon frequencies of ZA phonons are within the low frequencies of 0–30 THz, while the in-plane transverse and longitudinal phonons occupy much higher frequencies of 40–50 THz [35]. Therefore, the overall PDOS of graphene spreads widely from 0 to 50 THz. While for the phosphorene system, it has been proved that its PDOS has the same peak frequencies in all three directions within the frequencies of 0–15 THz [23]. Thus, phosphorene has a larger PDOS overlap with the bulk silicon system whose PDOS frequencies are mainly within 0–18 THz [54]. Larger overlap of PDOS indicates that more phonons in phosphorene system are involved in the interfacial thermal transport process than that of graphene, which results in a lower thermal contact resistance.

From our points of view, the higher sensitivity of R for phosphorene than silicene to environmental conditions originates from its peculiar hinge-like structure in the out-of-plane (z) direction. It is well-known that silicene has a slightly buckled structure of
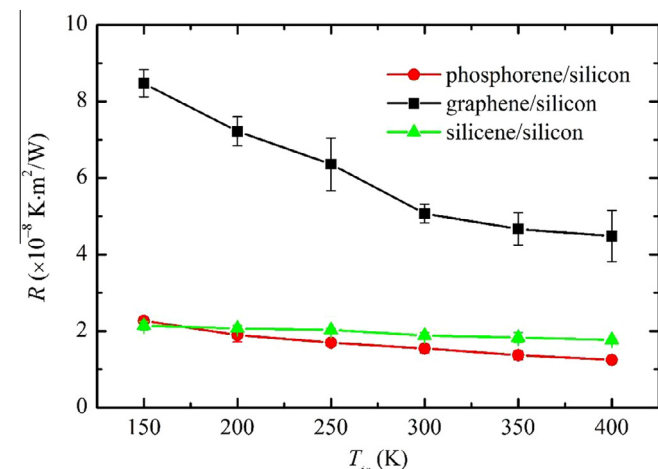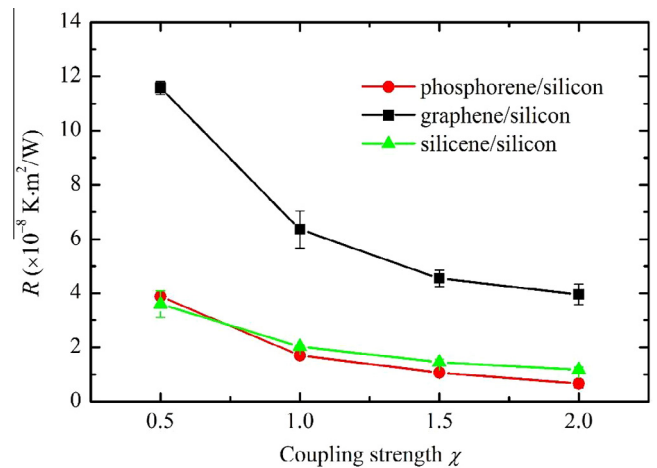

Fig. 10. Comparisons of R with respect to χ. The thermal contact resistance decreases monotonically with increasing coupling strength. The maximum decrease of R is calculated at 82.8%, 65.9% and 67.5% for phosphorene/silicon, graphene/silicon and silicene/silicon respectively.

~0.42 Å in the z direction [55]. While for phosphorene, the buckling distance has a much larger value of ~2.13 Å, which is more than 5 times larger than that of silicene. Therefore, when T_{ie} or χ increases, the lattice structures of phosphorene will be the more affected than those of silicene, which enhances the anharmonic phonon scatterings in the system and contribute to the change of R.

In summary, the above two extraordinary thermal characteristics, *i.e.*, low interfacial thermal resistance and high environmental sensitivity, demonstrate that phosphorene is an attractive candidate for the high-performance thermal interface materials.

5. Conclusion

The interfacial heat transfer across phosphorene and crystalline silicon was investigated using classical MD simulations. The Stillinger–Weber potential with first-principle calculated reliable parameters was employed to model the interactions among phosphorene atoms. It is found that when the system reaches steady state, the interfacial thermal resistance between phosphorene and silicon remains nearly constant and unaffected by the thickness of silicon substrate. The results also show that the interfacial thermal resistance between phosphorene and silicon decreases when the system temperature and coupling strength increase. The other remarkable findings are that under typical environmental conditions, the interfacial thermal resistance for phosphorene is only a quarter to that for graphene and more sensitive to the environmental variations than silicene. These two advantages indicate that phosphorene is a very promising high-performance externally-echoed 2D material for next-generation nano-devices.

Fig. 9. Comparisons of R with respect to temperature for phosphorene/silicon, graphene/silicon, and silicene/silicon. The error bars represent the standard deviation based on five independent simulations.

References

[1] K.K. Gomes, W. Mar, W. Ko, F. Guinea, H.C. Manoharan, Designer Dirac fermions and topological phases in molecular graphene, Nature 483 (7389) (2012) 306–310.
[2] L. Liao, Y.C. Lin, M.Q. Bao, R. Cheng, J.W. Bai, Y.A. Liu, Y.Q. Qu, K.L. Wang, Y. Huang, X.F. Duan, High-speed graphene transistors with a self-aligned nanowire gate, Nature 467 (7313) (2010) 305–308.

[3] A. Allain, J.H. Kang, K. Banerjee, A. Kis, Electrical contacts to two-dimensional semiconductors, Nat. Mater. 14 (12) (2015) 1195–1205.

[4] K.F. Mak, K.L. McGill, J. Park, P.L. McEuen, The valley Hall effect in MoS$_2$ transistors, Science 344 (6191) (2014) 1489–1492.

[5] X.B. Yin, Z.L. Ye, D.A. Chenet, Y. Ye, K. O'Brien, J.C. Hone, X. Zhang, Edge nonlinear optics on a MoS$_2$ atomic monolayer, Science 344 (6183) (2014) 488–490.

[6] J.J. Pei, X. Gai, J. Yang, X.B. Wang, Z.F. Yu, D.Y. Choi, B. Luther-Davies, Y.R. Lu, Producing air-stable monolayers of phosphorene and their defect engineering, Nat. Commun. 7 (2016) 10450.

[7] R.X. Fei, A. Faghaninia, R. Soklaski, J.A. Yan, C. Lo, L. Yang, Enhanced thermoelectric efficiency via orthogonal electrical and thermal conductances in phosphorene, Nano Lett. 14 (11) (2014) 6393–6399.

[8] Y.X. Deng, Z. Luo, N.J. Conrad, H. Liu, Y.J. Gong, S. Najmaei, P.M. Ajayan, J. Lou, X. F. Xu, P.D. Ye, Black phosphorus-monolayer MoS$_2$ van der Waals heterojunction p-n diode, ACS Nano 8 (8) (2014) 8292–8299.

[9] H. Wang, X.M. Wang, F.N. Xia, L.H. Wang, H. Jiang, Q.F. Xia, M.L. Chin, M. Dubey, S.J. Han, Black phosphorus radio-frequency transistors, Nano Lett. 14 (11) (2014) 6424–6429.

[10] Z.B. Yang, J.H. Hao, S.G. Yuan, S.H. Lin, H.M. Yau, J.Y. Dai, S.P. Lau, Field-effect transistors based on amorphous black phosphorus ultrathin films by pulsed laser deposition, Adv. Mater. 27 (25) (2015) 3748–3754.

[11] J.Q. He, D.W. He, Y.S. Wang, Q.N. Cui, M.Z. Bellus, H.Y. Chiu, H. Zhao, Exceptional and anisotropic transport properties of photocarriers in black phosphorus, ACS Nano 9 (6) (2015) 6436–6442.

[12] J. Zhang, X. Wang, H. Xie, Co-existing heat currents in opposite directions in graphene nanoribbons, Phys. Lett. A 377 (41) (2013) 2970–2978.

[13] C. Li, J. Zhang, X. Wang, Phase change and stress wave in picosecond laser–material interaction with shock wave formation, Appl. Phys. A 112 (3) (2013) 677–687.

[14] J. Zhang, F. Xu, Y. Hong, Q. Xiong, J. Pan, A comprehensive review on the molecular dynamics simulation of the novel thermal properties of graphene, RSC Adv. 5 (109) (2015) 89415–89426.

[15] Y. Yue, J. Zhang, X. Tang, S. Xu, X. Wang, Thermal transport across atomic-layer material interfaces, Nanotechnol Rev 4 (6) (2015) 533–555.

[16] J. Zhang, X. Wang, Thermal transport in bent graphene nanoribbons, Nanoscale 5 (2) (2013) 734–743.

[17] Y. Yue, J. Zhang, X. Wang, Micro/nanoscale spatial resolution temperature probing for the interfacial thermal characterization of epitaxial graphene on 4H-SiC, Small 7 (23) (2011) 3324–3333.

[18] P.N. Keating, Effect of invariance requirements on the elastic strain energy of crystals with application to the diamond structure, Phys. Rev. 145 (2) (1966) 637–645.

[19] J. Jin-Wu, Parametrization of Stillinger–Weber potential based on valence force field model: application to single-layer MoS$_2$ and black phosphorus, Nanotechnology 26 (31) (2015) 315706.

[20] M. Daniel, H.L. Caio, C. Alexander, Strain–displacement relations for strain engineering in single-layer 2d materials, 2D Mater. 3 (1) (2016) 011005.

[21] S. Zhen-Dong, P. Qing-Xiang, D. Zhiwei, J. Jin-Wu, Z. Yong-Wei, Mechanical properties and fracture behavior of single-layer phosphorene at finite temperatures, J. Phys. D Appl. Phys. 48 (39) (2015) 395303.

[22] Y.-Y. Zhang, Q.-X. Pei, J.-W. Jiang, N. Wei, Y.-W. Zhang, Thermal conductivities of single- and multi-layer phosphorene: a molecular dynamics study, Nanoscale 8 (1) (2016) 483–491.

[23] Y. Hong, J. Zhang, X. Huang, X.C. Zeng, Thermal conductivity of a two-dimensional phosphorene sheet: a comparative study with graphene, Nanoscale 7 (44) (2015) 18716–18724.

[24] H. Feng, L. Xiangbiao, X. Hang, C. Xi, Thermal conductivity of armchair black phosphorus nanotubes: a molecular dynamics study, Nanotechnology 27 (15) (2016) 155703.

[25] J. Tersoff, New empirical approach for the structure and energy of covalent systems, Phys. Rev. B 37 (12) (1988) 6991–7000.

[26] Y.H. Lin, T.C. Chen, P.F. Yang, S.R. Jian, Y.S. Lai, Atomic-level simulations of nanoindentation-induced phase transformation in mono-crystalline silicon, Appl. Surf. Sci. 254 (5) (2007) 1415–1422.

[27] W.C.D. Cheong, L.C. Zhang, Molecular dynamics simulation of phase transformations in silicon monocrystals due to nano-indentation, Nanotechnology 11 (3) (2000) 173–180.

[28] M. Posselt, F. Gao, H. Bracht, Correlation between self-diffusion in Si and the migration mechanisms of vacancies and self-interstitials: an atomistic study, Phys. Rev. B 78 (3) (2008) 035208.

[29] J. Zhang, Y. Wang, X. Wang, Rough contact is not always bad for interfacial energy coupling, Nanoscale 5 (23) (2013) 11598–11603.

[30] Z. Liang, H.-L. Tsai, Reduction of solid–solid thermal boundary resistance by inserting an interlayer, Int. J. Heat Mass Transf. 55 (11–12) (2012) 2999–3007.

[31] L. Zhi, T. Hai-Lung, Effect of thin film confined between two dissimilar solids on interfacial thermal resistance, J. Phys.: Condens. Matter 23 (49) (2011) 495303.

[32] Z. Liang, H.L. Tsai, Effect of interlayer between semiconductors on interfacial thermal transport, Proc. ASME Micro/Nanoscale Heat Mass Transfer Int. Conf. 2012 (2012) 335–344.

[33] A.K. Rappe, C.J. Casewit, K.S. Colwell, W.A. Goddard, W.M. Skiff, UFF, a full periodic table force field for molecular mechanics and molecular dynamics simulations, J. Am. Chem. Soc. 114 (25) (1992) 10024–10035.

[34] S. Plimpton, Fast parallel algorithms for short-range molecular dynamics, J. Comput. Phys. 117 (1) (1995) 1–19.

[35] J. Zhang, Y. Hong, Y. Yue, Thermal transport across graphene and single layer hexagonal boron nitride, J. Appl. Phys. 117 (13) (2015) 134307.

[36] Y. Xu, H. Wang, Y. Tanaka, M. Shimono, M. Yamazaki, Measurement of interfacial thermal resistance by periodic heating and a thermo-reflectance technique, Mater. Trans. 48 (2) (2007) 148–150.

[37] R. Kato, I. Hatta, Thermal conductivity and interfacial thermal resistance: measurements of thermally oxidized SiO$_2$ films on a silicon wafer using a thermo-reflectance technique, Int. J. Thermophys. 29 (6) (2008) 2062–2071.

[38] J.W. Pomeroy, R.B. Simon, H. Sun, D. Francis, F. Faili, D.J. Twitchen, M. Kuball, Contactless thermal boundary resistance measurement of GaN-on-diamond wafers, IEEE Electron Device Lett. 35 (10) (2014) 1007–1009.

[39] Y. Hong, L. Li, X.C. Zeng, J. Zhang, Tuning thermal contact conductance at graphene-copper interface via surface nanoengineering, Nanoscale 7 (14) (2015) 6286–6294.

[40] J. Zhang, X. Huang, Y. Yue, J. Wang, X. Wang, Dynamic response of graphene to thermal impulse, Phys. Rev. B 84 (23) (2011) 235416.

[41] M. Li, J. Zhang, X. Hu, Y. Yue, Thermal transport across graphene/SiC interface: effects of atomic bond and crystallinity of substrate, Appl. Phys. A 119 (2) (2015) 415–424.

[42] R.X. Su, Z.Q. Yuan, J. Wang, Z.G. Zheng, Enhanced energy transport owing to nonlinear interface interaction, Sci. Rep. 6 (2016) 19628.

[43] N.M. Pugno, Q.F. Yin, X.H. Shi, R. Capozza, A generalization of the Coulomb's friction law: from graphene to macroscale, Meccanica 48 (8) (2013) 1845–1851.

[44] L.J. Wang, Q.K. Li, Z. Shuai, Effects of pressure and temperature on the carrier transports in organic crystal: a first-principles study, J. Chem. Phys. 128 (19) (2008) 194706.

[45] J.-L. Barrat, F. Chiaruttini, Kapitza resistance at the liquid–solid interface, Mol. Phys. 101 (11) (2003) 1605–1610.

[46] T.Q. Vo, B. Kim, Interface thermal resistance between liquid water and various metallic surfaces, Int. J. Precis. Eng. Manuf. 16 (7) (2015) 1341–1346.

[47] L. Xue, P. Keblinski, S.R. Phillpot, S.U.-S. Choi, J.A. Eastman, Two regimes of thermal resistance at a liquid–solid interface, J. Chem. Phys. 118 (1) (2003) 337–339.

[48] B.H. Kim, A. Beskok, T. Cagin, Molecular dynamics simulations of thermal resistance at the liquid–solid interface, J. Chem. Phys. 129 (17) (2008) 174701.

[49] W.B. Donald, A.S. Olga, A.H. Judith, J.S. Steven, N. Boris, B.S. Susan, A second-generation reactive empirical bond order (REBO) potential energy expression for hydrocarbons, J. Phys.: Condens. Matter 14 (4) (2002) 783.

[50] L. Lindsay, D.A. Broido, Optimized Tersoff and Brenner empirical potential parameters for lattice dynamics and phonon thermal transport in carbon nanotubes and graphene, Phys. Rev. B 81 (20) (2010) 205441.

[51] T. Kumagai, S. Izumi, S. Hara, S. Sakai, Development of bond-order potentials that can reproduce the elastic constants and melting point of silicon for classical molecular dynamics simulation, Comput. Mater. Sci. 39 (2) (2007) 457–464.

[52] J. Zhang, Y. Hong, Z. Tong, Z. Xiao, H. Bao, Y. Yue, Molecular dynamics study of interfacial thermal transport between silicene and substrates, Phys. Chem. Chem. Phys. 17 (37) (2015) 23704–23710.

[53] J. Zhang, X. Wang, H. Xie, Phonon energy inversion in graphene during transient thermal transport, Phys. Lett. A 377 (9) (2013) 721–726.

[54] L. Hai-peng, Z. Rui-qin, Vacancy-defect? induced diminution of thermal conductivity in silicene, EPL (Europhysics Letters) 99 (3) (2012) 36001.

[55] Z. Ni, Q. Liu, K. Tang, J. Zheng, J. Zhou, R. Qin, Z. Gao, D. Yu, J. Lu, Tunable bandgap in silicene and germanene, Nano Lett. 12 (1) (2012) 113–118.